ADVANCED ENGINEERING MATERIALS
www.aem-journal.com

Check for updates

RuAl Thin-Film Deposition by DC Magnetron Sputtering

Vincent Ott, Tomasz Wojcik, Szilard Kolozsvari, Peter Polcik, Christian Schäfer, Christoph Pauly, Frank Mücklich, Sven Ulrich, Paul H. Mayrhofer, Helmut Riedl, and Michael Stüber*

The intermetallic transition metal B2-structured aluminide RuAl is a candidate material for use in various applications, including microelectronics and structural materials under demanding conditions, for example, as oxidation- and corrosion-resistant materials. In contrast to other B2 transition metal aluminides, which usually suffer from brittle material behavior at room temperature, RuAl exhibits comparatively good room-temperature ductility, in combination with further promising properties. Therefore, RuAl thin films are attracting interest as potential protective and functional surface engineering materials. The synthesis of RuAl thin films by physical vapor deposition, especially magnetron sputtering, is however complex and utilizes codeposition and multilayer from elemental sputtering targets and subsequent annealing procedures. Herein, an alternative route toward single-phase B2-structured RuAl thin films by nonreactive DC magnetron sputter deposition at low substrate temperature from a powdermetallurgically manufactured $Ru_{50}Al_{50}$ compound target is described. The influence of the deposition parameters on the constitution, microstructure, and selected properties of RuAl thin films is studied. It is shown that especially the Ar process gas pressure has a significant impact on their composition and morphology. X-ray diffraction and transmission electron microscopy with selected-area electron diffraction indicate that the films are single-phase RuAl with B2 structure.

1. Introduction

Considering material solutions for highly demanding applications, aluminide intermetallics have found significant and increasing importance in various areas over the past decades. They are well known for interesting property profiles, covering, for example, high melting points, mechanical strength, good electric, and thermal conductivity and excellent corrosion resistance. The related binary phase diagrams are complex and multiple materials constitutions and microstructures are known for aluminides. Applications of high-performance materials based on advanced Ni superalloys and TiAl alloys are state of the art for example in aircraft industries. However, aluminides face also multiple challenges: Although they are commonly used as an additive in composite materials, their usage as bulk materials is often hindered by their poor manufacturing ability due to their brittle behavior at room temperature (RT).[1,2]

Among the huge variety of transition metal aluminides, phases like NiAl, CoAl, and FeAl with B2 structure with base centered cubic-like symmetry are in the focus of diverse research studies as approaching alternative high-temperature materials.[3–5] Among those B2 aluminides, RuAl has attracted huge interest due to a ductile–brittle temperature below RT. RuAl crystallizes in the cubic CsCl structure, consisting of two interlaced cubic primitive sublattices (space group $Pm\bar{3}m$), where each Al atom is surrounded only by Ru atoms (and vice versa). The resulting strong bonding with covalent contribution determines its mechanical properties. In 1992, Fleischer compared various intermetallic bulk compounds in B2 and L10 structure.[6] A density of 7.97 g cm^{-3} was reported, lower than the density of Ni-based superalloys.[7] The mechanical properties of bulk samples showed a Young's modulus of

V. Ott, S. Ulrich, M. Stüber
Institute for Applied Materials
Karlsruhe Institute of Technology
Hermann-von-Helmholtz-Platz 1, 76344 Eggenstein-Leopoldshafen, Germany
E-mail: vincent.ott@kit.edu

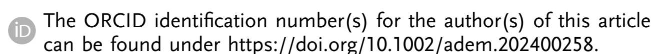
The ORCID identification number(s) for the author(s) of this article can be found under https://doi.org/10.1002/adem.202400258.

© 2024 The Author(s). Advanced Engineering Materials published by Wiley-VCH GmbH. This is an open access article under the terms of the Creative Commons Attribution-NonCommercial License, which permits use, distribution and reproduction in any medium, provided the original work is properly cited and is not used for commercial purposes.

DOI: 10.1002/adem.202400258

T. Wojcik, P. H. Mayrhofer, H. Riedl
Institute of Materials Science and Technology
TU Wien
Getreidemarkt 9, 1060 Wien, Austria

S. Kolozsvari, P. Polcik
Plansee Composite Materials GmbH
Siebenbürgerstraße 23, 86983 Lechbruck am See, Germany

C. Schäfer, C. Pauly, F. Mücklich
Functional Materials
Saarland University
Campus D3 3, 66123 Saarbrücken, Germany

 © 2024 The Author(s). Advanced Engineering Materials published by Wiley-VCH GmbH

267 GPa and good RT ductility along with a melting point of 2060 °C.[8] Special attention was paid to specific strength as well as to the melting point and the elastic behavior at RT and elevated temperatures. Investigations on the microhardness of bulk RuAl and alloyed, isostructural (Ru,Ni)Al by Sabariz and Taylor showed values of ≈310 HV for pure RuAl and considerably increasing values with the addition of the alloying element (Ni).[9] Further studies on the improvement of the mechanical properties of RuAl discussed an enhanced ductility for an additional alloying with 0.5 at% boron.[10] Fleischer pointed out further that compositional changes of RuAl within the homogeneity range of the B2 RuAl phase have an impact on the mechanical properties. He showed that this effect can be used to specifically tune the properties of bulk RuAl. It was, for example, demonstrated that an over-stoichiometric Al content in RuAl resulted in a strong reduction of plasticity. With increasing Ru content in RuAl, the ductility increased progressively up to the maximum Ru concentration (50.6 at%) of the RuAl phase.[8] The mechanical properties of RuAl were related to the line defect structure of the RuAl phase. Transmission electron microscopy (TEM) studies of bulk RuAl alloys in the annealed condition revealed clearly the presence of dislocations with Burgers vectors along <100>, <110>, and <111> directions.[8] The majority of these dislocations were observed on {110} planes and exhibited <100> and <110> Burgers vectors as shown by Lu and Pollock.[11] The comparatively high-RT ductility of RuAl allowing a strain rate of 10% is superior compared to other aluminides and is attributed to the presence of a sufficient number of slip systems.[12] A comprehensive description of the RuAl phase and Ru–Al phase diagram, combining both experimental and simulation data, has been presented by Mücklich et al. The authors discussed in detail the atomistic structure and the derived materials characteristics in terms of electrical and mechanical properties.[13,14]

Apart of its promising mechanical properties, the main advantage of RuAl resides in its oxidation behavior. Inward diffusion of oxygen and inverted Al diffusion lead to an opaque α-Al_2O_3 formation hindering further oxidation of the material.[15–18] In addition, the thermal expansion coefficients of the RuAl phase and the α-Al_2O_3 are very close to each other.[19] Heating the material above a threshold temperature of 850 °C leads to the formation of volatile Ru oxides in the Ru-rich interlayer being formed, causing the spallation of the Al_2O_3 layer.[20] Below this critical operating temperature, novel applications of RuAl become accessible, for example, its use as a metallization layer in surface acoustic wave sensors.[21–23]

The synthesis of Ru–Al materials, and especially of stoichiometric RuAl, is not trivial, and different processing technologies are considered for this purpose. Melting metallurgical production to achieve exact composition of the Ru–Al material is complicated due to the high vapor pressure of Al at the melting point of Ru.[24] Increased attention has therefore been paid to powder metallurgical processes (and mechanical alloying routes) and as well to thin-film deposition, mainly using physical vapor deposition (PVD) techniques.

Considering powder metallurgically-based methods to synthesize RuAl, the study of self-propagating reactions or self-propagating high-temperature synthesis (SHS) has been studied in detail. These processes make use of the fact that the formation of the intermetallic phase RuAl is strongly exotherm, with a negative enthalpy of formation of $-62.4\,kJ\,mol^{-1}$.[25] Without further referring to details, the SHS synthesis of bulk RuAl has been addressed by Povarova for different Ru–Al alloys. Such powder metallurgical samples often show the occurrence of pores, which have a negative influence on the mechanical properties.[26] This is partially a result of the application of reactive sintering processes and is facilitated by the aforementioned negative enthalpy of formation. On the other hand, mechanical alloying provides an alternative, reliable method for the synthesis of the RuAl phase.[27–30]

A new path to synthesize Ru–Al-based materials and to possibly explore their full technical potential is their synthesis in the form of thin films and coatings. Up to date, only few experimental studies have been published hereon, indicating however clearly the strength of the methods toward achieving high-quality crystalline B2-structured RuAl thin films for functional and protective applications. The preferred technique used for this purpose is magnetron sputtering. The major approaches utilized encompass the simultaneous codeposition of Ru and Al from elemental targets[31,32] or the alternating deposition of Ru and Al in nanoscale multilayer architectures.[33–35] In both cases, the desired intermetallic RuAl phase is formed by a subsequent heat treatment.[34,36–38] Considering phase formation in thin films prepared by codeposition of elemental Ru and Al, rapid thermal annealing to about 800 °C is usually used to assist the RuAl phase formation.[32,39,40]

Recently, we have demonstrated that the nanoscale architecture of magnetron-sputtered Ru/Al multilayers and the subsequent annealing procedure have a significant impact on phase formation. Using tailored multilayer designs and annealing procedures, the Ru/Al multilayers can transform directly from the elemental layers into the desired single-phase RuAl thin films, without any intermediate reaction product.[41] It should be noted, that in such nanoscale multilayer thin films, the above-mentioned self-propagating exothermic reactions can again be initiated and used for phase formation.[21] By controlling the Al/Ru ratio, the resulting intermetallic phase of the binary Al/Ru system can be determined.[36,42–44]

In this work, we discuss another, alternative route to synthesize RuAl thin films via magnetron sputtering from a single-compound target with the desired composition of each 50 at% Ru and Al. This method has not been described in detail, and only very few reports are available. For example, Yang et al. used nanoscale RuAl thin films up to 20 nm as seed layer to control the grain growth of magnetic FePt coatings.[45–47] In our present study, we show how the variation of process parameters in the magnetron sputtering process, composition, constitution, microstructure, and selected properties of the as-deposited Ru–Al thin films, can be adjusted and fine tuned. The focus of this manuscript is on the description of the synthesis of crystalline B2-structured RuAl thin films at low substrate temperature by magnetron sputtering from a solid compound target without requiring a thermal annealing-induced phase formation.[34,36–38]

2. Results and Discussion

The preliminary investigations showed that the most relevant parameter in the thin-film synthesis of RuAl is the argon gas

© 2024 The Author(s). Advanced Engineering Materials published by Wiley-VCH GmbH

15272648, 0, Downloaded from https://onlinelibrary.wiley.com/doi/10.1002/adem.202400258 by Karlsruher Institut F., Wiley Online Library on [27/06/2024]. See the Terms and Conditions (https://onlinelibrary.wiley.com/terms-and-conditions) on Wiley Online Library for rules of use; OA articles are governed by the applicable Creative Commons License

pressure during the coating process. The other parameters such as the power or the substrate bias voltage also showed an influence, though no major impact could be observed. Based on the five different Ar gas pressures used for the deposition of the Ru–Al thin films (the other deposition parameters were not varied), these five different samples were investigated with respect to their chemistry, growth morphology, growth rate, microstructure, and mechanical properties.

2.1. Thin-Film Deposition, Growth Rate, and Composition

Figure 1 shows the RuAl target voltage (for a constant DC power of 250 W) and growth rate of the Ru–Al thin films upon the Ar gas pressure variation during deposition.

The target voltage decreases continuously with increasing Ar gas pressure, from 420 V at 0.1 Pa to 350 V at 2.0 Pa. This effect is commonly known for the sputtering of homogeneous metallic targets and is based on the increase of the number of ionized Ar-atoms with increasing pressure reducing the required voltage to maintain the glow discharge.[48] Vice versa, the growth rate of the Ru–Al thin films increases slightly but noticeably by 10% with increasing Ar gas pressure. This effect is discussed in combination with the results obtained for the thin film composition, **Figure 2**. The Ru–Al thin films exhibit only low impurities concentrations for oxygen, carbon, nitrogen, or argon, which all together are in the range 1.2–2.3 at%. These impurities are statistically present (without a noticeable correlation with the Ar gas pressure) in the different thin films and are not further considered for the following discussion. Figure 2 shows also the maximum Ru content of the B2 RuAl phase according to the phase diagram of Mücklich and Ilic (indicated by the horizontal dashed line).[13] The minimum Ru content for this phase is at RT at ≈47 at%. All deposited Ru–Al thin films, except the one deposited at 0.1 Pa, exhibit a chemical composition within these boundaries. The Ru–Al thin films show a variation in their Ru/Al composition from 50.6/48.2 at% when prepared at 0.1 Pa Ar pressure to 48.7/48.9 at% when prepared at 2.0 Pa Ar pressure (absolute concentrations). This corresponds to 51.2/48.8 at% and 49.9/50.1 at% when normalized to solely Ru + Al. For the normalized Ru content also the thin film prepared at 0.4 Pa Ar pressure would exhibit a slightly higher Ru content (51.0/49.0 at%) in comparison to the given maximum RT limit of 50.6 at% for the RuAl phase. However, sputtering is a well-known nonequilibrium process allowing for phase compositions beyond the given limits of equilibrium phase diagrams.

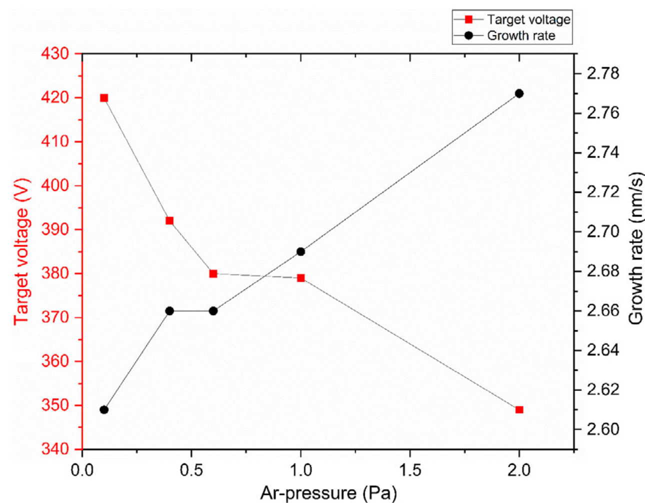

Figure 1. Resulting negative target voltage at 250 W applied DC power and the growth rate of the Ru–Al thin films versus the Ar pressure.

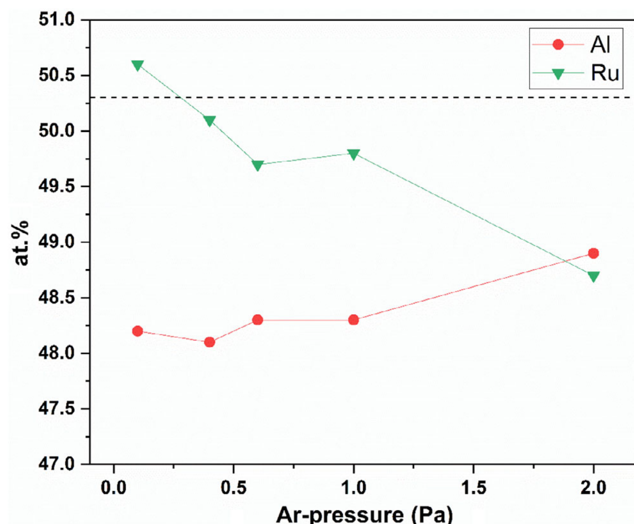

Figure 2. Concentrations of metallic elements of Ru–Al thin films, determined by EPMA. The dashed line indicates the theoretical maximum Ru content in the RuAl phase at RT according to Mücklich and Ilic.[13]

The variation in chemistry with the Ar gas pressure can be rationalized with the characteristics of sputtering, that is, with the angular distribution of sputtered species, the scattering effects, as well as film formation processes of the Ru and Al species. Considering a steady-state sputtering condition of the target—which is typically valid especially for nonreactive processes—the sputtering ratio between Ru and Al is 1, regardless of the Ar gas pressure. However, the angular distribution of sputtered species between Ru and Al is different, leading to different arrival rates at certain substrate positions, even if both elements would have similar scattering effects with the process gas.

A similar effect is known for the nonreactive sputter deposition of other materials, such as TiB_2, when the ceramic diboride target consists of a light and a heavy element, B and Ti. The lighter element (B) is preferentially sputtered along the target surface normal, while the heavier element (Ti) leaves the target in a significantly wider angular range from the target surface normal (under specific conditions of the magnetic field configuration in the PVD chamber).[49,50] This effect might be similar for the sputtering of the RuAl target, where the significantly heavier element (Ru) should exhibit a wider sputter angle distribution with respect to the target surface normal.[51,52] This would explain differences in the composition of the Ru–Al thin films being deposited on the sapphire substrates positioned centrally opposite to the target. The maximum Al content is therefore to be expected directly opposite the magnetron sputter race-track, but as the substrates are shifted relative to this, this effect should be

© 2024 The Author(s). Advanced Engineering Materials published by Wiley-VCH GmbH

15272648, 0, Downloaded from https://onlinelibrary.wiley.com/doi/10.1002/adem.202400258 by Karlsruher Institut F., Wiley Online Library on [27/06/2024]. See the Terms and Conditions (https://onlinelibrary.wiley.com/terms-and-conditions) on Wiley Online Library for rules of use; OA articles are governed by the applicable Creative Commons License

negligible. Increasing the Ar gas pressure decreases the mean free path of the sputtered species, resulting in an increased number of collisions normalizing the different sputter angle distribution.[53] Further, selective resputtering effects of the film-forming species can lead to different chemical compositions and composition variations with the variation of the Ar gas pressure. For example, investigations of W–Ti films by Shaginyan et al. show that the lighter atoms (Ti) are preferentially resputtered form the forming thin-film surface through the impact of the heavier energetic particle (W). Increasing the Ar pressure lowers the kinetic energy of the sputtered species due to collisions in the transport phase and thereby these resputtering effects decrease as well as the energy of the impacting W species decreases.[54] Similarly, this effect could contribute to our observation of an increased growth rate with increasing Ar pressure. However, plasma diagnostics and the simulation of deposition physics in the Ru–Al system as well as atomistic modeling of possible resputtering effects could provide further insights into the processes.

2.2. Growth Morphology and Microstructure

The X-ray diffraction (XRD) analyses show that all films are crystalline, single-phase B2 RuAl with a strong preferential growth, perpendicular to the (110) lattice plane (Figure S1, Supporting Information). With increasing Ar pressure, there is a shift of the diffraction reflections toward higher angles (Figure S2, Supporting Information), which at the same time indicates a reduction in the lattice parameter derived from the (110) lattice plane parallel to the surface of the RuAl phase (see **Figure 3**). The results of the phase analysis were confirmed by XRD measurements in grazing incidence. This implies that the lattice parameter systematically decreases with increasing Ar pressure and vice versa with decreasing Ru concentration and increasing Al concentration (see Figure 2). This observation is in contrast to the investigations of Gobran et al. who showed a linear increase of the lattice parameters with decreasing Ru content on equilibrium annealed RuAl samples.[55] For the small variation of the Ru content shown in this work, the lattice parameter would change by 0.002 Å according to Gobran et al. which is negligible with regard to the shift caused by microstructural and stress-induced effects. In relation to the reference value of 2.992 Å for stoichiometric B2 RuAl reported by Fleischer et al. this work shows larger values for the lattice parameters of the Ru–Al layers, which were deposited at pressures up to 1 Pa.[56] For the coatings deposited at 2.0 Pa, the measured values in this work correspond to the literature value. Therefore, the shift of the peaks with increasing Ar pressure toward higher angles during deposition (in the range of 0.1°) should be correlated with the presence of decreasing intrinsic stresses due to lowering in particle energy of the adatoms, caused by the higher Ar pressure.

A detailed evaluation of the thin-film structure and microstructure was obtained by TEM analyses. For this purpose, the Ru–Al thin-film samples deposited at 0.4 and 2.0 Pa Ar pressure were selected for further investigations.

2.2.1. Ru–Al Thin Films Deposited at 0.4 Pa Ar Pressure

XRD analysis indicates that the analyzed film exhibits a single-phase B2 RuAl structure, **Figure 4**, with a strongly preferred (110) growth orientation. Next to this most pronounced XRD peak at $2-\theta = 42.60°$ only two additional peaks (attributable to the RuAl-phase) can be detected, the (210) at $2-\theta = 69.86°$ and the (211) at $2-\theta = 77.87°$. The XRD peak positions are slightly shifted to lower diffraction angles compared to the indicated reference state (RuAl: ICDD PDF, # 04-003-2136).[56] Therefore, a pole figure of this respective diffraction reflection was prepared and compared to the sputter condition of 2.0 Pa Ar pressure—please see Figure 7 and the related discussion. A clearly pronounced textured structure with lattice planes in (110) orientation, parallel to the surface of the thin film, is observed and appears to be only very slightly tilted against the surface normal vector. This implies that there are only very small deviations from the preferred growth orientation and relatively

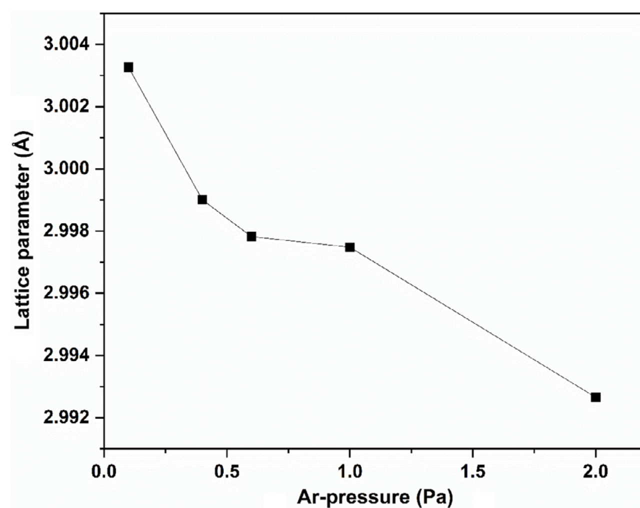

Figure 3. Lattice parameter of the RuAl thin films sputtered at different Ar pressures.

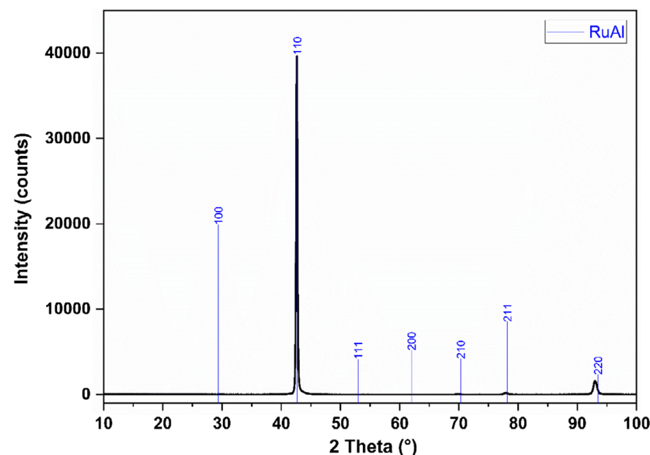

Figure 4. X-ray diffractogram of a RuAl film deposited at 0.4 Pa Ar pressure. The blue lines mark the theoretical intensities and angular positions of the reflections of B2 RuAl phase normalized to the peak of highest intensity.

© 2024 The Author(s). Advanced Engineering Materials published by Wiley-VCH GmbH

15272648, 0, Downloaded from https://onlinelibrary.wiley.com/doi/10.1002/adem.202400258 by Karlsruher Institut F., Wiley Online Library on [27/06/2024]. See the Terms and Conditions (https://onlinelibrary.wiley.com/terms-and-conditions) on Wiley Online Library for rules of use; OA articles are governed by the applicable Creative Commons License

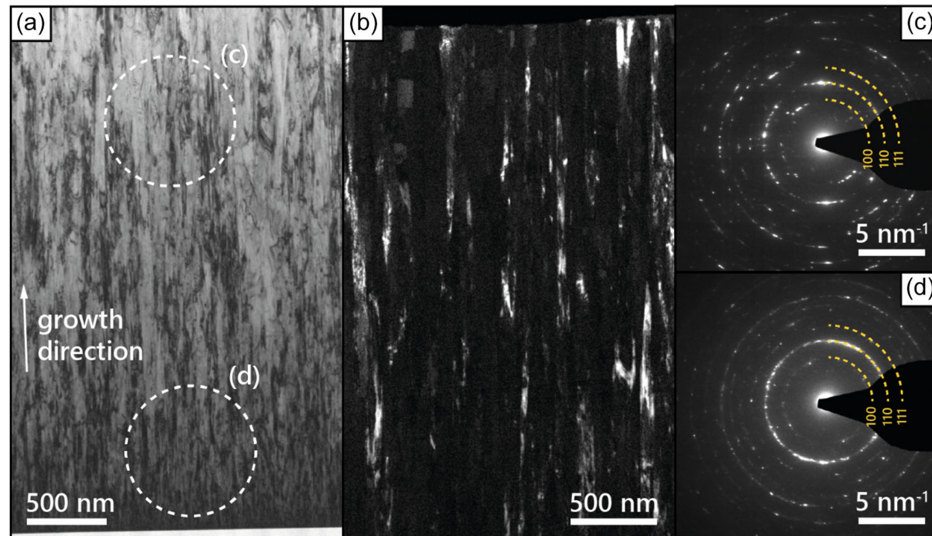

Figure 5. TEM investigation of a cross-sectional RuAl thin-film sample (thin film deposited at 250 W and 0.4 Pa Argon). a) Bright-field image, b) dark-field image, c) SAED pattern of the region c) marked by the white dotted circle in (a,d). d) SAED pattern of the region marked by the white dotted circle in a).

strict energetic advantages for incorporating the adatoms into this lattice plane.

The cross-sectional TEM analysis, **Figure 5**, shows a fine-grained, dense fibrous growth morphology. At the interface to the sapphire substrate, the width of the elongated fibrous grains is much smaller. In average, the width of the columns increases to 31 ± 9 nm in the surface near area and their length easily extends to 1 µm, see the dark-field TEM image taken on a (110) reflection, Figure 5b. The increasing columnar grain size with increasing coating thickness is nicely reflected with the corresponding selected-area electron diffraction (SAED) patterns, Figure 5c,d, respectively. The regions shown in these patterns are indicated by white dotted circles in Figure 5a, describing thin-film cross-section areas near the film–substrate interface and in a position closer to the film surface. Both SAED patterns solely exhibit the B2 RuAl phase. In the substrate-near thin-film region, the corresponding SAED pattern (Figure 5d) shows almost continuous diffraction rings consisting of very fine diffraction spots that are evenly distributed along the rings. Meanwhile, closer to the surface (region (c) in Figure 5a), the reflections in the SAED pattern are more pronounced due to the larger crystallite sizes and accumulated at specific orientations. Moderate texturing with the (110) reflection parallel to the growth direction is observed.

2.2.2. Ru–Al Thin Films Deposited at 2.0 Pa Ar Pressure

The XRD analysis of a film deposited at a high Ar pressure of 2.0 Pa, **Figure 6**, is rather similar to that of the film prepared at a low Ar pressure of 0.4 Pa, Figure 4. The preferred growth orientation is still a pronounced (110), but now with additional small intensity for the (100) orientation as well (at $2-\theta$ angles of 29.85° for (100) and 61.85° for (200)). The shift of the XRD peaks toward higher angles is even more pronounced for thin films prepared at 2.0 Pa Ar pressure than for those prepared at 0.4 Pa Ar

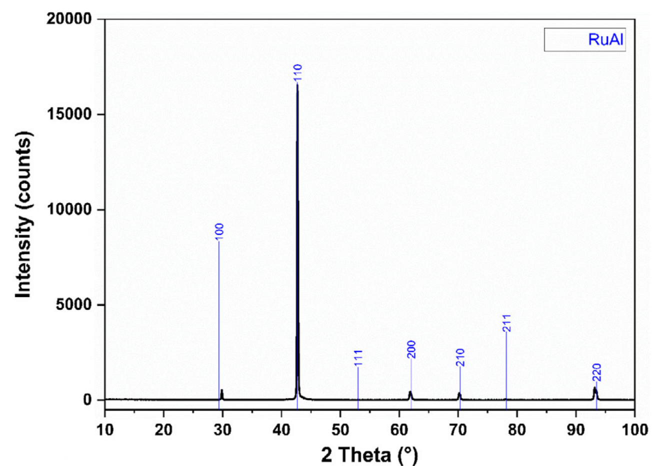

Figure 6. X-ray diffractogram of a RuAl film deposited at 2.0 Pa Ar pressure. The blue lines mark the theoretical intensities and angular positions of the reflections of B2 RuAl phase normalized to the peak of highest intensity.

pressure. A comparison of both films, which show a pronounced (110) growth orientation, was conducted with the help of pole figure measurements, see **Figure 7**a,b, respectively. The film prepared at lower Ar pressure exhibits more pronounced textured orientation of the lattice planes in (110) orientation. The grains are only slightly tilted away from the surface normal vector. Thus, only some grains deviate from the preferred (110) growth orientation. In addition, four symmetrically arranged reflections can be identified (marked with "S" in Figure 7a, which can be assigned to the substrate, as this has a diffraction reflection at a very similar $2-\theta$ angle. The film prepared at the higher Ar pressure still shows a pronounced (110) growth orientation, but here more grains deviate from this, leading to additional XRD reflections.

© 2024 The Author(s). Advanced Engineering Materials published by Wiley-VCH GmbH

15272648, 0, Downloaded from https://onlinelibrary.wiley.com/doi/10.1002/adem.202400258 by Karlsruher Institut F., Wiley Online Library on [27/06/2024]. See the Terms and Conditions (https://onlinelibrary.wiley.com/terms-and-conditions) on Wiley Online Library for rules of use; OA articles are governed by the applicable Creative Commons License

15272648, 0, Downloaded from https://onlinelibrary.wiley.com/doi/10.1002/adem.202400258 by Karlsruher Institut F., Wiley Online Library on [27/06/2024]. See the Terms and Conditions (https://onlinelibrary.wiley.com/terms-and-conditions) on Wiley Online Library for rules of use; OA articles are governed by the applicable Creative Commons License

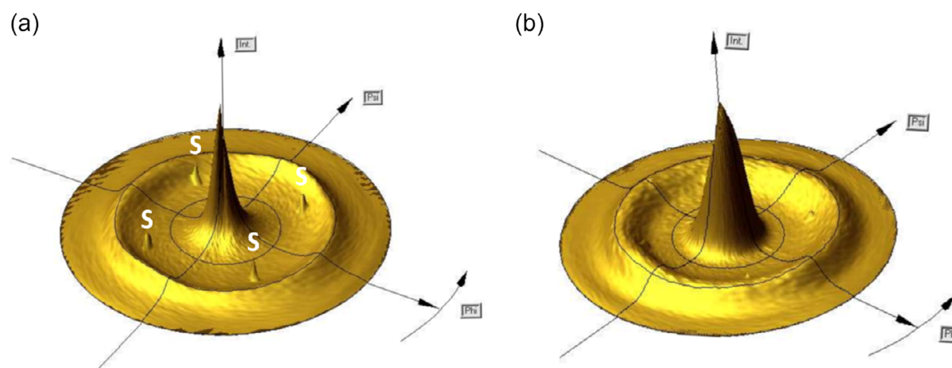

Figure 7. Pole figures of the diffraction reflection of the (110) orientation of RuAl thin films deposited at 250 W and a) 0.4 Pa and b) 2.0 Pa argon.

Compared to the film prepared at lower Ar pressure, the one prepared at 2.0 Pa Ar pressure exhibits a more coarse-grained columnar growth morphology, **Figure 8**. Also here, the column width is much smaller (several nm) at the interface region to the sapphire substrate and becomes wider along the film thickness (with 71 ± 33 nm close to the surface). The dark-field image on a (110) reflection, Figure 8b, nicely shows the column lengths easily extend over 1 μm, similar to the film prepared at lower Ar pressure. Again, the SAED patterns taken from a cross-sectional area closer to the film surface, Figure 8c, exhibit a more spot-like characteristic due to the rather long crystals (longer than the aperture size), which are well aligned. Close to the interface to the sapphire substrate, the SAED pattern is more ring like (Figure 8d), as here the columnar grains are smaller.

The growth morphology of the RuAl thin films represents a competitive growth, leading to the formation of V-shaped crystallites. Starting from more random nucleation sites at the sapphire substrates, the fast-growing low-energy (110)-oriented grains overgrow the others. Thereby, the columnar width increases from the interface near region toward the film surface. Furthermore, the observation of overall larger crystallites for the film prepared at higher Ar pressure is in line with the previous conclusion from the concomitant increased Al content and deposition rate. Due to the increased scattering of sputter species for increased Ar pressure, their energy is reduced, and they will impact the film forming surface with lower energy. Thereby, the lighter Al species are less likely resputtered (therefore the Ru/Al ratio decreases toward 1 upon increasing the Ar pressure, see Figure 2), the growth rate increases, and the film forming crystals are less damaged. The latter results in reduced renucleation events and therefore the films prepared at higher Ar pressure are coarser grained. This effect also fits well with Thornton's structural zone model as well as the revised model according to Anders.[57,58]

2.3. Mechanical Properties of the RuAl Thin Films

The RT indentation hardness values of the as-deposited magnetron sputtered RuAl thin films are between 11.5 and 13.6 GPa

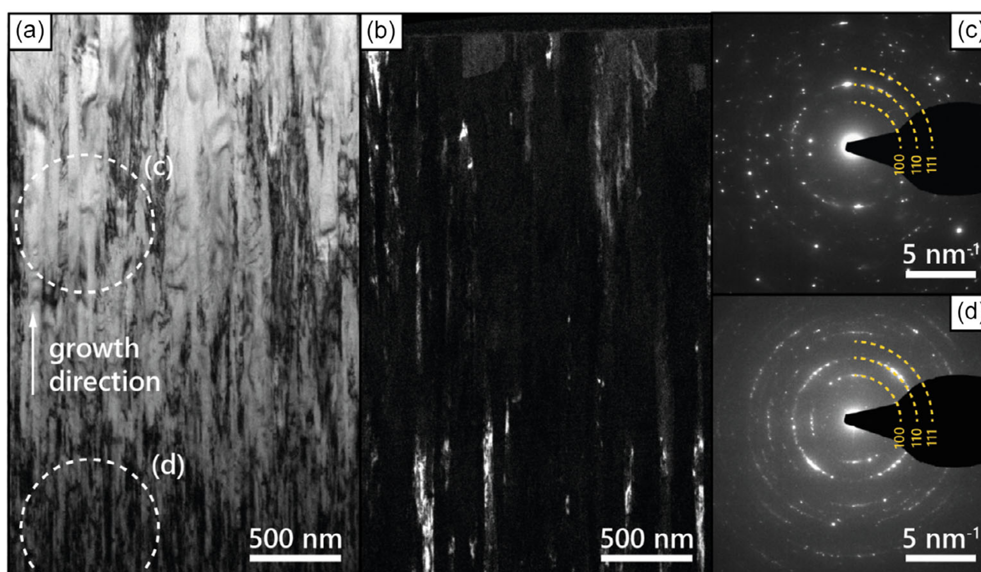

Figure 8. TEM investigation of a cross-sectional RuAl thin-film sample (thin film deposited at 250 W and 2.0 Pa Argon). a) Bright-field image, b) dark-field image, c) SAED pattern of the region c) marked by the white dotted circle in (a,d). d) SAED pattern of the region marked by the white dotted circle in (a).

© 2024 The Author(s). Advanced Engineering Materials published by Wiley-VCH GmbH

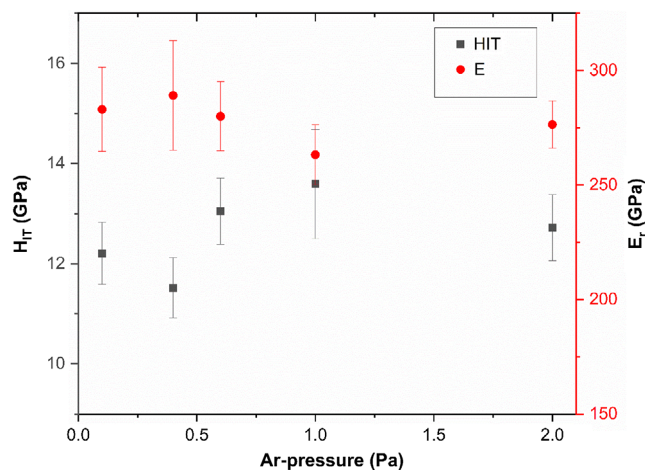

Figure 9. Dependence of the indentation hardness as well as the reduced Young's modulus on the Ar pressure during coating.

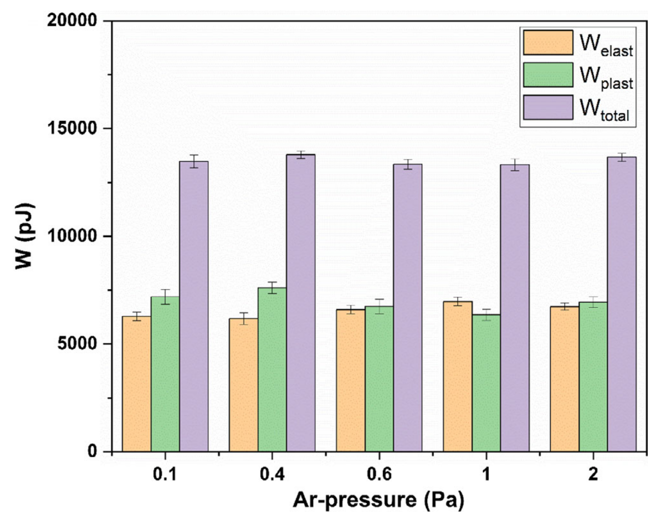

Figure 10. Elastic, plastic, and total deformation energy of the RuAl thin films applied for microindentation with 100 mN.

(see **Figure 9**). These values are significantly larger than those known for corresponding RuAl bulk materials exhibiting typical hardness of 3-4 GPa. Such a difference is frequently observed when thin films and bulk materials are compared, for example, also in case NiAl.[59] No trend can however be observed with respect to an influence of the different nanoscale columnar microstructures of the Ru–Al thin-film samples on the hardness values. In the case of the RuAl films of this study, there may be a superposition of different effects, leading to an increase in hardness of the thin films compared to the bulk value. For example, the alignment of the (110) lattice planes parallel to the layer surface can influence the hardness additionally. Considering the crystallographic system and the results of the dislocation structure analysis by Fleischer et al. most of the dislocations are lying on these most densely packed (110) planes.[8] Since the largest stresses under normal load occur at a 45° angle, an increase in hardness can be explained by texturation, leading to anisotropic mechanical behavior. Furthermore, the nanoscale microstructures of the thin films lead to a high number of defects in the form of grain boundaries and dislocations.[60] These hinder the dislocation movement, which leads to a reduced plastic deformation and increases the hardness.[61] In addition, there is a further increase due to residual stresses, which often occur in sputtered thin films.[62] Although this parameter was not explicitly determined in this work, the shift of the XRD reflections of the as-deposited RuAl thin films toward lower angles indicates residual compressive stresses in the coatings, potentially contributing to the high hardness. With respect to the reduced Young's modulus, all specimens show a similar value between 289 and 263 GPa. These values are in good agreement with the bulk value of 267 GPa.[8] Again, no explicit trend in the E_r values for the thin-film samples deposited at different pressures can be observed.

In addition to the H_{IT} and E_r values, the applied strain energy during indentation experiments was estimated by evaluation of the indentation curves. These results can be divided into an elastic and plastic fraction by determining the integral values under the specific parts of the indentation curves. The derived values give an impression of the type of deformation under the load of 100 mN and can be considered as an indicator of the ductility of the particular thin film. **Figure 10** shows the elastic, plastic, and total deformation energy of the indentations for RuAl thin films in relation with the Ar gas pressure during deposition. All measurements show very similar values for the total energy, but also for the respective proportions of the plastic and elastic strain energy. The proportion of plastic strain energy and the total energy varies between 0.48 and 0.55, from which a certain RT ductility of the RuAl thin films can be derived.

3. Conclusion

The deposition of single-phase RuAl thin films in the B2 structure can be synthesized by DC magnetron sputtering from a powder metallurgical target. This is demonstrated for a wide variation of the gas pressure during deposition between 0.1 and 2.0 Pa argon (while other parameters such as substrate temperature, substrate bias, and DC target power were kept constant). The variation of the gas pressure corresponds with a systematic change of the mean free path of the sputtered species between the target and the substrate. In consequence, and in correlation with the physics of the sputter behavior of solid compound targets containing heavy and light weight elements and the angular distribution of the sputter ejected species, the elemental composition of the RuAl thin films can be tuned on a very fine scale from 50.6/48.2 at% at 0.1 Pa to 48.7/48.9 at%. at 2.0 Pa. This indicates that the deposition process is robust, reproducible, and can be tailored. At the same time, a reduction in the lattice parameters with increasing working gas pressure is evident. In addition to a reduction in the Ru content (with a simultaneous increase in the Al content), increasing the Ar pressure also leads to the formation of a coarser microstructure with all of the samples showing a strong preferential growth of RuAl grains in (110) orientation. This effect evolves with the thin-film thickness, starting with a smaller-grained polycrystalline microstructure in the substrate-near areas. An influence of the compositional changes on the

© 2024 The Author(s). Advanced Engineering Materials published by Wiley-VCH GmbH

15272648, 0, Downloaded from https://onlinelibrary.wiley.com/doi/10.1002/adem.202400258 by Karlsruher Institut F., Wiley Online Library on [27/06/2024]. See the Terms and Conditions (https://onlinelibrary.wiley.com/terms-and-conditions) on Wiley Online Library for rules of use; OA articles are governed by the applicable Creative Commons License

RT mechanical properties of the respective thin films could not be demonstrated in this study, which is in contrast to the state of knowledge on bulk material. At the same time, all thin films exhibit a significantly higher hardness than is known for bulk material, but with similar Young's modulus values. The synthesis process described in this work can provide single-phase B2 RuAl thin films in one step, without the need of a subsequent heat treatment. As a result, we obtain comparatively different microstructures with regard to the grain structure and the observed preferred orientation of thin films that have been synthesized by postannealing of precisely designed nanoscale Ru/Al multilayer thin films or codeposited coatings.[32,34,35,63] This allows to deposit RuAl thin films on temperature-sensitive substrate materials and with a tailored microstructure.

4. Experimental Section

The thin-film deposition was carried out by nonreactive DC magnetron sputtering in a Leybold Z550 laboratory-scale coating system. The system enabled thin films to be deposited under different conditions with regard to the plasmaphysical processes during sputtering. The sputtering target used was a cylindrical disk with a diameter of 75, 5 mm thickness, and a 50/50 at% composition of Ru/Al, bonded to a water-cooled copper backing plate.

The target was powder mechanically manufactured from elemental, not-alloyed aluminum, and ruthenium powders with an average grain size below 50 μm. Densification of Ru–Al ingots, used for target manufacturing, was performed by subsequently applied pressing and forging at a maximum temperature in the range of 400 °C to avoid formation of any intermetallic phases, so that the obtained material was a composite of ruthenium grains embedded into an aluminum matrix and was not alloyed. Metallic purity of the material was 99.9% and the density above 95% of the theoretical density.

Homogeneously grown thin films of ≈4 μm total thickness were deposited in a top-down process with a target to substrate distance of 50 mm. The substrates (polished single-crystal sapphire substrates ($10 \times 10 \times 1$ mm^3) with a c-orientation) were not additionally heated, resulting in temperatures during the deposition in the range 80–120 °C (due to plasma interactions). After reaching a base pressure of $\leq 2 \times 10^{-6}$ mbar, the RuAl target was sputter cleaned (against a shutter) for 3 min at 250 W DC target power in an Ar (purity 6.0) discharge. Prestudies showed that when a substrate bias potential was used, the thin films exhibited high residual stresses, leading to local spallation. For all thin-film samples discussed in this work, no substrate bias was applied during deposition, and the substrates were even grounded, that is, at zero potential.

The films were investigated with electron probe microanalysis (EPMA) for their chemical composition. A Cameca SX 100 system was operated with 15 keV acceleration voltage and 30 nA current. On each sample, 3 different surface areas were analyzed, and the values reported for the chemical composition were the average of these measurements. The investigations were performed by wavelength-dispersive X-ray spectroscopy using different analyzer crystals (PET, PC2 and PC80) and standard samples as references (TiN, ArSi 10, TiC, YiG, AlFe-Rank, G12Ni, and TiB2).

Phase analysis and microstructure characterization was done by XRD with a Panalytical Empyrean (operated with 40 kV and 40 mA) in Bragg–Brentano geometry using Cu Kα radiation ($\lambda = 1.540598$ Å). The step size of the measurement was 0.0131° with a measuring time of 150 s per step. A PIXCEL3D Medipix3 1×1 was used as a 1D line detector, which allowed a measurement range of 3.347° to be evaluated simultaneously. The $2-\theta$ range covered in these measurements was 10°–100°. The irradiated length of the sample was fixed to a length of 8 mm by the automatic divergence slit. The assessment of the XRD raw data was performed via the Highscore software using the ICCD PDF4+ database. Information on phase composition, crystallinity, crystalline structure, orientation, and texture formation was obtained. Pole figures for the investigation of textures or preferred orientations were realized using a five-axis sample holder. The diffraction reflection position of the peak to be examined in the Bragg–Brentano geometry was used for the determination and the angle of incidence on the sample was fixed accordingly. The sample was then tilted in 1° steps from its horizontal position up to 90°. At each step, a diffractogram was recorded during a 360° rotation around the sample normal.

Cross-sectional lamellas for TEM analysis were cut out using a Thermo Fisher SCIOS 2 focused ion beam device. TEM investigations were carried out on an FEI Tecnai F20 equipped with a field-emission gun and operated at 200 kV acceleration voltage. Bright-field and dark-field images revealed the microstructure of the coatings. SAED patterns were analyzed with CrystBox[64] to study the crystal structure and texture, based on the primitive cubic RuAl phase (space group 221) with a lattice constant $a = 0.2992$ nm.[56] The lattice constant was estimated from high-resolution TEM micrographs by averaging over ten distances of lattice fringes.

To determine the elastic modulus, indentation hardness, and the elastic and plastic strain energies of the thin films, a CSM micro-combi tester of type MCT was used. The indentations were performed according to the Oliver and Pharr method. Load–displacement curves were recorded in the load-controlled operation mode. The maximum load of the Vickers indenter was 100 mN. For each sample, 9 analyses were done and the results reported in this study were averaged values of these individual analyses. The elastic and plastic strain energies were derived from the integral values of the respective parts of the resulting indentation curves.

Supporting Information

Supporting Information is available from the Wiley Online Library or from the author.

Acknowledgements

Main parts of this work and the corresponding author were funded by the Deutsche Forschungsgemeinschaft (DFG, German Research Foundation)—426339194. The authors thank the University Service Centre for Transmission Electron Microscopy at TU Wien for providing TEM facilities.

Open Access funding enabled and organized by Projekt DEAL.

Conflict of Interest

The authors declare no conflict of interest.

Data Availability Statement

The data that support the findings of this study are available from the corresponding author upon reasonable request.

Keywords

intermetallics, magnetron sputtering, ruthenium aluminides

Received: January 31, 2024
Revised: May 21, 2024
Published online:

[1] M. Yamaguchi, H. Inui, K. Ito, *Acta Mater.* **2000**, *48*, 307.
[2] S. H. Whang, D. P. Pope, C. T. Liu, in *High Temperature Aluminides and Intermetallics: Proceedings of the Second Int. ASM Conf. on High Temperature Aluminides and Intermetallics, September 16–19, 1991, San Diego, CA, USA*, Elsevier, London **1992**.

© 2024 The Author(s). Advanced Engineering Materials published by Wiley-VCH GmbH

15272648, 0, Downloaded from https://onlinelibrary.wiley.com/doi/10.1002/adem.202400258 by Karlsruher Institut F., Wiley Online Library on [27/06/2024]. See the Terms and Conditions (https://onlinelibrary.wiley.com/terms-and-conditions) on Wiley Online Library for rules of use; OA articles are governed by the applicable Creative Commons License

[3] H. Clemens, S. Mayer, *MSF* **2016**, *879*, 113.
[4] K. Bochenek, M. Basista, *Prog. Aerospace Sci.* **2015**, *79*, 136.
[5] F. Hadef, *Powder Technol.* **2017**, *311*, 556.
[6] R. L. Fleischer, *Platinum Met. Rev.* **1992**, *36*, 138.
[7] R. L. Fleischer, R. J. Zabala, *MTA* **1990**, *21*, 2709.
[8] R. L. Fleischer, R. D. Field, C. L. Briant, *MTA* **1991**, *22*, 403.
[9] A. L. R. Sabariz, G. Taylor, *MRS Proc.* **1996**, *460*, 611.
[10] R. L. Fleischer, *Acta Mater.* **2005**, *53*, 2623.
[11] D. C. Lu, T. M. Pollock, *MRS Proc.* **1998**, *552*, 7111.
[12] K. Gschneidner, A. Russell, A. Pecharsky, J. Morris, Z. Zhang, T. Lograsso, D. Hsu, C. H. C. Lo, Y. Ye, A. Slager, D. Kesse, *Nat. Mater.* **2003**, *2*, 587.
[13] F. Mücklich, N. Ilić, *Intermetallics* **2005**, *13*, 5.
[14] F. Mücklich, N. Ilić, K. Woll, *Intermetallics* **2008**, *16*, 593.
[15] M. Seifert, G. K. Rane, S. Oswald, S. B. Menzel, T. Gemming, *Materials* **2017**, *10*, 277.
[16] M. Seifert, G. K. Rane, S. B. Menzel, S. Oswald, T. Gemming, *J. Alloys Compd.* **2019**, *776*, 819.
[17] J. A. Howell, C. L. Muhlstein, B. Z. Liu, Q. Zhang, S. E. Mohney, *J. Microelectromech. Syst.* **2011**, *20*, 933.
[18] P. J. Bellina, *PhD Thesis, High temperature oxidation of bulk RuAl alloy*, Universität Stuttgart, **2006**.
[19] B. Tryon, T. M. Pollock, M. Gigliotti, K. Hemker, *Scr. Mater.* **2004**, *50*, 845.
[20] P. J. Bellina, A. Catanoiu, F. M. Morales, M. Rühle, *J. Mater. Res.* **2006**, *21*, 276.
[21] M. Seifert, B. Leszczynska, S. B. Menzel, H. Schmidt, T. Gemming, *J. Mater. Res. Technol.* **2023**, *26*, 1955.
[22] M. Seifert, E. Brachmann, G. K. Rane, S. B. Menzel, S. Oswald, T. Gemming, *J. Alloys Compd.* **2020**, *813*, 152107.
[23] A. Karimzadeh, E. Park, M. Seifert, S. B. Menzel, A. Winkler, *Adv. Mater. Technol.* **2023**, *8*, 2201979.
[24] T. Reynolds, D. Johnson, *MRS Proc.* **2004**, *842*, 423.
[25] S. N. Prins, L. A. Cornish, W. E. Stumpf, B. Sundman, *Calphad* **2003**, *27*, 79.
[26] K. B. Povarova, A. E. Morozov, A. A. Drozdov, A. V. Antonova, M. A. Bulakhtina, *Inorg. Mater. Appl. Res.* **2021**, *12*, 1125.
[27] S. N. de Medeiros, F. Machado, R. B. Zampiere, I. A. Santos, A. Paesano, *J. Non-Cryst. Solids* **2006**, *352*, 3718.
[28] A. Borah, P. S. Robi, A. Srinivasan, *Met. Mater. Int.* **2007**, *13*, 293.
[29] K. W. Liu, F. Mücklich, *Acta Mater.* **2001**, *49*, 395.
[30] K. Liu, F. Mücklich, R. Birringer, *Intermetallics* **2001**, *9*, 81.
[31] W. K. Shen, J. H. Judy, J.-P. Wang, *J. Appl. Phys.* **2005**, *97*, 10H301.
[32] M. Seifert, S. B. Menzel, G. K. Rane, M. Hoffmann, T. Gemming, *Mater. Res. Express* **2015**, *2*, 85001.
[33] K. Woll, R. Chinnam, F. Mücklich, *MRS Proc.* **2008**, *1128*, 610.
[34] N. Zotov, K. Woll, F. Mücklich, *Intermetallics* **2010**, *18*, 1507.
[35] M. A. Guitar, H. Aboulfadl, C. Pauly, P. Leibenguth, S. Migot, F. Mücklich, *Surf. Coat. Technol.* **2014**, *244*, 210.
[36] K. Woll, *PhD Thesis, Festkörper- und selbstfortschreitende Reaktionen in Multilagen zur RuAl-Dünnschichtsynthese*, Universität des Saarlandes Saarbrücken **2012**.
[37] R. Haikal, *Egypt. J. Solids* **2009**, *32*, 89.
[38] Z. A. Chaudhury, C. Suryanarayana, *J. Mater. Sci.* **1982**, *17*, 3158.
[39] Y.-Y. Fang, Y.-H. Tsai, Y.-L. Chen, D.-J. Jhan, M.-Y. Lu, P. Y. Keng, S.-Y. Chang, *Appl. Phys. Lett.* **2024**, *124*, 142108.
[40] J. A. Howell, S. E. Mohney, C. L. Muhlstein, *J. Vac. Sci. Technol. B* **2011**, *29*, 042002.
[41] V. Ott, C. Schäfer, S. Suarez, K. Woll, F. Mücklich, H. J. Seifert, S. Ulrich, C. Pauly, M. Stueber, *Coatings* **2023**, *13*, 149.
[42] C. Pauly, *PhD Thesis, Selbstfortschreitende Reaktionen in Ru/Al/X-Multilagen*, Universität des Saarlandes, Saarbrücken **2017**.
[43] C. Pauly, K. Woll, B. Bax, F. Mücklich, *Appl. Phys. Lett.* **2015**, *107*, 113104.
[44] H. Aboulfadl, F. Mücklich, *Mater. Lett.* **2019**, *254*, 344.
[45] E. Yang, S. Ratanaphan, J.-G. Zhu, D. E. Laughlin, *J. Appl. Phys.* **2011**, *109*, 07B770.
[46] E. Yang, S. Ratanaphan, D. E. Laughlin, J.-G. Zhu, *IEEE Trans. Magn.* **2011**, *47*, 81.
[47] E. Yang, H. Ho, J.-G. Zhu, D. E. Laughlin, *IEEE Trans. Magn.* **2011**, *47*, 4077.
[48] G. Buyle, D. Depla, K. Eufinger, J. Haemers, W. Bosscher, R. Gryse, *Vacuum* **2004**, *74*, 353.
[49] I. Petrov, A. Hall, A. B. Mei, N. Nedfors, I. Zhirkov, J. Rosen, A. Reed, B. Howe, G. Greczynski, J. Birch, L. Hultman, J. E. Greene, *J. Vac. Sci. Technol. A* **2017**, *35*, 050601.
[50] J. Neidhardt, S. Mráz, J. M. Schneider, E. Strub, W. Bohne, B. Liedke, W. Möller, C. Mitterer, *J. Appl. Phys.* **2008**, *104*, 063304-1.
[51] R. Behrisch, W. Eckstein, in *Sputtering by Particle Bombardment: Experiments and Computer Calculations from Threshold to MeV Energies*, Springer, Berlin **2007**.
[52] N. Mahne, M. Čekada, M. Panjan, *Coatings* **2022**, *12*, 1541.
[53] E. Särhammar, T. N. Nicolas Martin, *Int. J. Mater. Sci. Appl.* **2014**, *3* 29.
[54] L. R. Shaginyan, M. Mišina, S. Kadlec, L. Jastrabík, A. Macková, V. Peřina, *J. Vac. Sci. Technol. A* **2001**, *19*, 2554.
[55] H. A. Gobran, D. Heger, F. Mücklich, *Int. J. Mater. Res.* **2005**, *96*, 794.
[56] R. L. Fleischer, *Acta Metall. Mater.* **1993**, *41*, 863.
[57] A. Anders, *Thin Solid Films* **2010**, *518*, 4087.
[58] J. A. Thornton, *J. Vac. Sci. Technol.* **1975**, *12*, 830.
[59] Y. Ding, Y. Zhang, D. O. Northwood, A. T. Alpas, *Surf. Coat. Technol.* **1997**, *94–95*, 483.
[60] P. Panjan, A. Drnovšek, P. Gselman, M. Čekada, M. Panjan, *Coatings* **2020**, *10*, 447.
[61] E. Broitman, *Tribol. Lett.* **2017**, *65*, 23.
[62] G. Abadias, E. Chason, J. Keckes, M. Sebastiani, G. B. Thompson, E. Barthel, G. L. Doll, C. E. Murray, C. H. Stoessel, L. Martinu, *J. Vac. Sci. Technol. A* **2018**, *36*, 020801.
[63] M. A. Guitar, K. Woll, E. Ramos-Moore, F. Mücklich, *Thin Solid Films* **2013**, *527*, 1.
[64] M. Klinger, A. Jäger, *J. Appl. Crystallogr.* **2015**, *48*, 2012.

© 2024 The Author(s). Advanced Engineering Materials published by Wiley-VCH GmbH

15272648, 0, Downloaded from https://onlinelibrary.wiley.com/doi/10.1002/adem.202400258 by Karlsruher Institut F., Wiley Online Library on [27/06/2024]. See the Terms and Conditions (https://onlinelibrary.wiley.com/terms-and-conditions) on Wiley Online Library for rules of use; OA articles are governed by the applicable Creative Commons License